Real-Time Carbon Content Control for PECVD ZrO_2 Thin-Film Growth

Dong Ni, Yiming Lou, Panagiotis D. Christofides, Lin Sha, Sandy Lao, and Jane P. Chang

***Abstract*—We present a methodology for real-time control of thin-film carbon content in a plasma-enhanced metal-organic chemical vapor deposition process using combination of online gas phase measurements obtained through optical emission spectroscopy and off-line (*ex situ*) measurements of film composition obtained via X-ray photoelectron spectroscopy (XPS). Initially, an estimation model of carbon content of ZrO_2 thin films based on real-time optical emission spectroscopy data is presented. Then, a feedback control scheme, which employs the proposed estimation model and a proportional-integral controller, is developed to achieve carbon content control. Using this approach, a real-time control system is developed and implemented on an experimental electron cyclotron resonance high-density plasma-enhanced chemical vapor deposition system to demonstrate the effectiveness of real-time feedback control of carbon content. Experimental results of depositions and XPS analysis of deposited thin films under both open-loop and closed-loop operations are shown and compared. The advantages of operating the process under real-time feedback control in terms of robust operation and lower carbon content are demonstrated.**

***Index Terms*—Carbon content, OES, PECVD, real-time feedback control, thin-film growth, XPS, ZrO_2.**

I. Introduction

THE decrease of microelectronic device dimensions has motivated the replacement of silicon dioxide with oxides of higher dielectric constant (κ) as a dielectric layer in metal oxide semiconductor (MOS) devices. This is because for silicon dioxide layers thinner than about 1.6 nm, direct tunnelling currents through the oxide result in an exponential increase of leakage current. Significant leakage current increases the power dissipation and deteriorates the device performance and circuit stability for very large scale integrated (VLSI) circuits [1], [2]. In addition, since the minimum dimension of capacitors for 1–4-Gb dynamic random access memory (DRAM) generations falls into the deep submicron range, it is questionable whether acceptable charge storage can be achieved with SiO_2 within such small size regime.

The alternative is to use layers of a "new" high-κ dielectric, with the same equivalent oxide thickness or capacitance. A large number of high-κ candidate materials have been extensively studied. Among these candidate materials, ZrO_2 (as well as HfO_2) has several important properties which make it a leading candidate for an alternative dielectric. The dielectric constant of ZrO_2 is relatively high among the binary-metal oxides ($\kappa \sim 25$), and its thermal stability on Si is very good. Moreover, studies have indicated that pure ZrO_2 next to Si (with an ultrathin intervening SiO_x layer) remains stable up to 900 °C [3]. In addition, ZrO_2 films have superior chemical resistance, good mechanical strength, and a low-leakage current level.

A variety of techniques can be used to prepare metal oxide thin films. Plasma-enhanced chemical vapor deposition (PECVD) is one of the most prominent means of preparing dielectric thin films, especially for memory devices applications, because of such advantages as low process temperature, high film growth rate, and wide flexibility of deposition conditions. The use of metal-organic (MO) chemicals as precursors in PECVD of metal oxide thin films enables uniform film growth over large areas and complex surface geometries. However, a potential problem of using MO precursors is the possibility of incorporation of impurities in the deposited thin film. One of the most important impurity species is carbon, which is abundant in the precursors. The incorporation of high concentration of carbon in the deposited film can adversely influence device performance by changing the dielectric constant and the leakage current density [4].

In general, carbon can be incorporated in the films either by forming carbides or oxides with the deposited metal or oxygen or by occupying intergranular positions among the grains of the main deposited compound in the form of cyclic or aliphatic species. Carbon incorporation can even occur simultaneously in multiple states depending on precursor, material to-be-deposited, and operating conditions [5], [6]. Therefore, the development and implementation of real-time feedback control systems for carbon content control could improve the operation and use of MO precursors in the deposition of high-κ materials.

Previous research on control of deposition processes has addressed control of film thickness in PECVD silicon epitaxy [10] and control of deposition spatial uniformity in PECVD amorphous silicon growth [7] (see also [8] for results on feedback control of plasma etching and [9] for results on feedback control of rapid thermal processing, as well as [17] and [18] for results on feedback control of thin film surface roughness). Recently, a method for real-time control of PECVD silicon nitride film properties for a relatively simple deposition chemistry was proposed in [11]; in this work, thin-film properties were indirectly controlled by regulating gas phase species compositions. At this stage, direct control of PECVD thin film properties has not been reported due to the complexity of both plasma physics and plasma chemistry and the difficulty to obtain real-time measurements of film properties.

Manuscript received April 22, 2003; revised December 23, 2003. This work was supported in part by the National Science Foundation (ITR) under Grant CTS-0325246

D. Ni, Y. Lou, and P. D. Christofides are with the Process Control Group, University of California, Los Angeles, CA 90095 USA (e-mail: pdc@seas.ucla.edu).

L. Sha, S. Lao, and J. P. Chang are with the Electronic Materials Synthesis and Plasma Processing Lab, University of California, Los Angeles, CA 90095 USA (e-mail: jpchang@ucla.edu).

Digital Object Identifier 10.1109/TSM.2004.826939

0894-6507/04$20.00 © 2004 IEEE

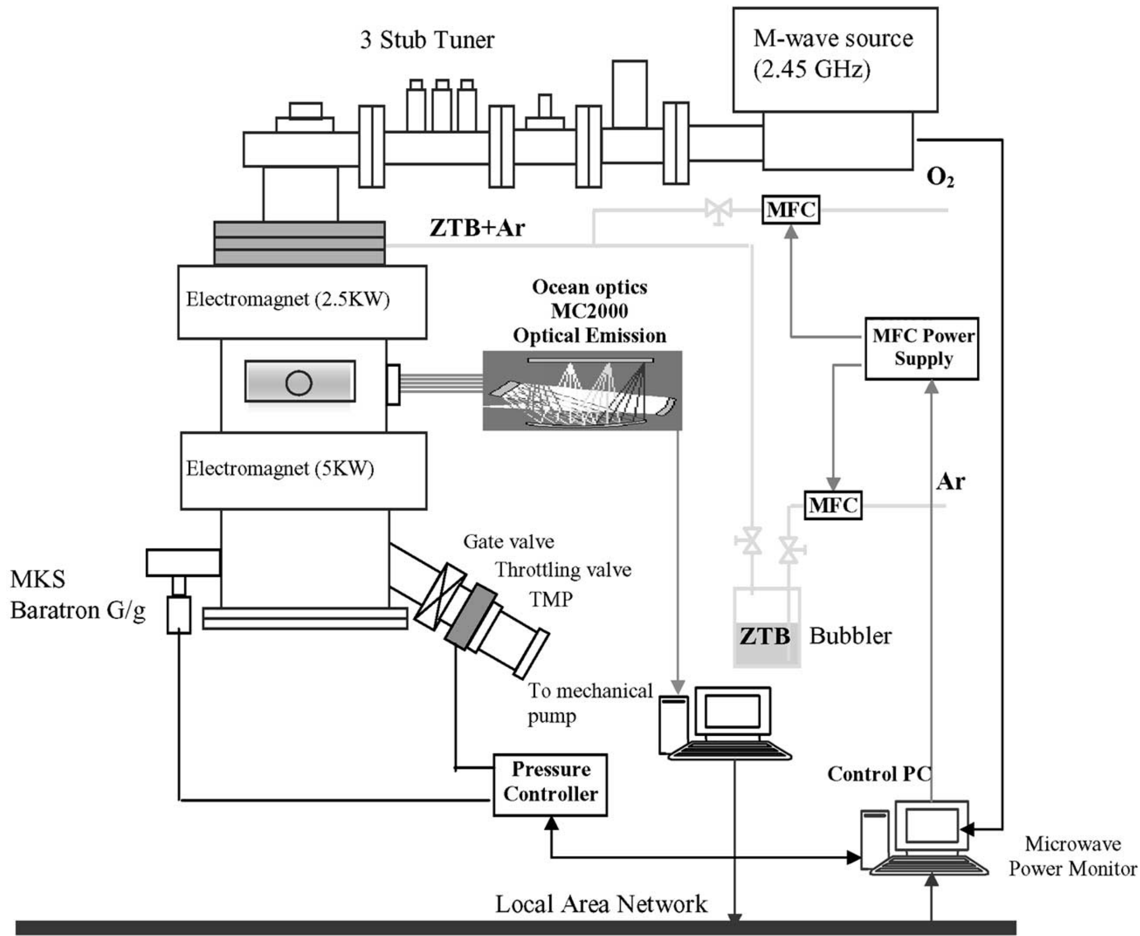

Fig. 1. Schematic diagram of the ECR PECVD system.

Optical emission spectroscopy (OES) has been widely used to monitor the gas phase species concentrations [12]. Moreover, OES has been used as measurement sensor for closed-loop control to regulate process variables such as the partial pressure of gas phase species [13], [14], and the film thickness based on empirical correlations [14]. However, although many researchers have suggested that OES signals could be utilized to control material properties such as thin-film composition [15], [16], no work has been done to design and implement a real-time feedback control system using combination of OES real-time measurements and off-line X-ray photoelectron spectroscopy (XPS) measurements to directly control the thin film composition and to verify the closed-loop performance by characterization of the deposited thin films.

In this work, we present a methodology for real-time control of thin-film carbon content in a plasma-enhanced metal-organic chemical vapor deposition process using combination of on-line gas phase measurements obtained through OES and off-line (*ex situ*) measurements of film composition obtained via XPS. The method is used for real-time control of carbon content of ZrO_2 thin films. Initially, an estimation model of carbon content of ZrO_2 thin films based on real-time optical emission spectroscopy data is presented. Then, a feedback control scheme, which employs the proposed estimation model and a proportional-integral controller, is developed to achieve carbon content control. Using this approach, a real-time control system is developed and implemented on an experimental electron cyclotron resonance (ECR) high-density PECVD system to demonstrate the effectiveness of real-time feedback control of carbon content. Experimental results of depositions and XPS analysis of deposited thin films under both open-loop and closed-loop operations are shown and compared. The advantages of operating the process under real-time feedback control in terms of robust operation and lower carbon content are demonstrated.

II. ECR High-Density PECVD Reactor

The schematic of the experimental ECR PECVD reactor system is shown in Fig. 1. It consists of an ECR type microwave source, a reactor chamber, a pumping system, a pressure control system, a gas delivery system, an OES system, and a computer-based real-time process control system.

Fig. 2 shows the internal configuration of the reactor chamber. A 6-in-diameter cylindrical stainless-steel chamber is surrounded by two circular coaxial electromagnets, which are 7 in apart. An ASTeX ECR source is on top of the chamber. Microwave at 2.45 GHz is generated from the source and transmitted into the chamber through a $3/8$-in-thick vacuum-sealed quartz window and a high-density plasma is generated. A gas diffusion ring is located just below the top quartz window to conduct uniform distribution of the gases. A 4-in-diameter anodized aluminum substrate holder is centered inside the

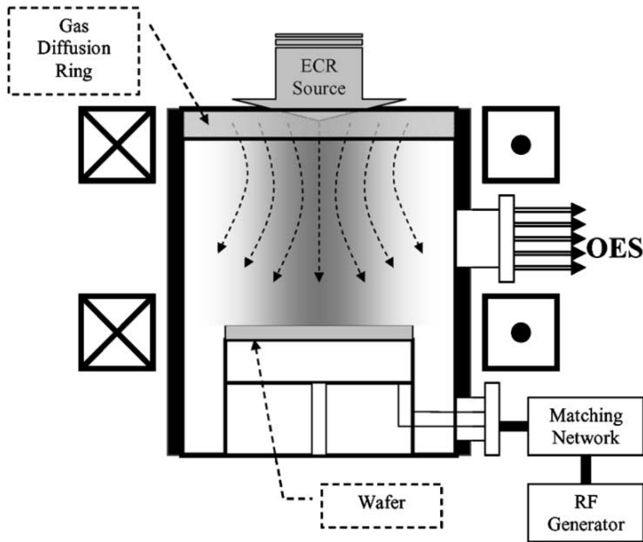

Fig. 2. Internal configuration of ECR PECVD chamber.

chamber. The distance between the substrate holder and the top quartz window is adjustable in the range of 6.5 to 12 in. The substrate holder is also connected with a 13.56-MHz radio frequency (RF) power supply tuned by a matching network; this allows for controlling the ion impinging energy by applying bias voltage to the substrate.

The chamber is pumped by a 140 l/s Alcatel 5150CP turbomolecular pump (TMP) backed by a mechanical pump. The base pressure is measured with an HPS I-Mag cold cathode ion gauge. The chamber pressure can be controlled and varied between the base pressure and atmospheric pressure. The MKS 651C pressure controller takes the measurement of chamber pressure by an MKS 626A Baratron gauge as input and manipulates an MKS 253B throttle valve, thereby allowing us to control the pressure independently from the gas flow rates.

We chose zirconium tetra-tert-butoxide [$Zr(OC_4H_9)_4$] (ZTB) as our MO precursor because it has a sufficiently high vapor pressure (0.26 mbar at 60 °C) [19]. A bubbler, which is kept at constant temperature (65 °C), is used for precursor delivery because ZTB is a liquid at room temperature (boiling point = 90 °C). Ar is used as a carrier gas of the precursor vapor and the gas line is heated to 80 °C to prevent the condensation of precursors. O_2 is used as an oxidant and mixed with Ar and ZTB at a point 8 in away from the entrance to the reactor.

Throughout this study, the electric currents are fixed at 120 A for the 5 kW top magnet and 150 A for the 2.5 kW bottom magnet. The distance between the top quartz window and the substrate holder is kept constant at 6.5 in and no bias is applied to the substrate.

III. Optical Emission Spectroscopy System

OES is the central real-time measurement tool used in this study. We use an Ocean Optics MC2000 OES system with five channels covering the wavelength range from 200 to 1000 nm to analyze the plasma. Each channel consists of independent optic setups including slits, gratings, a 2048-element linear silicon charged coupled diode (CCD) array, and an optic fiber cable. The configurations of individual channels are shown in Table I. The best optical resolution [full width at half maximum (FWHM)] for this system is 1.4 Å with a 10-μm slit width in the ultraviolet (UV) range. The integration time can be set within the range of 3 ms to 60 s. A sapphire window with minimal UV absorption is used as the OES port. The transmittance of the window does not vary significantly during each deposition run and the window is cleaned regularly to prevent accumulation of material on chamber walls. The emission spectra are taken 1 in above the substrate surface in this study so that gas phase information near the wafer surface can be collected.

TABLE I
Optical Emission Spectroscopy (OES) Channel Configurations of Wavelength Range, Start Pixel (SP), End Pixel (EP), and Resolution (in FWHM)

CH	Range (nm)	SP	EP	Res.[FWHM]
0	196.14 ~ 354.44	4	2044	1.5 Å
1	327.23 ~ 464.27	0	2047	1.4 Å
2	437.93 ~ 617.89	0	2047	1.8 Å
3	585.70 ~ 868.81	0	2046	2.8 Å
4	786.50 ~ 1039.51	1	2047	2.5 Å

TABLE II
Transitions and Wavelengths of Atomic Emissions Observed [23]

Species	Wavelength (nm)	Transition
Ar	750.39	$4s'_{(1/2)}{}^o - 4p'_{(1/2)}$
C	247.85	$2p^2\,{}^1S - 3s^1\,{}^4P^o$
H_β	486.13	$2p^2P^o - 4d^2D$
O	777.42	$3s^5S^o - 3p^5P$
Zr	350.93	N/A
	351.96	
Zr^+	339.20	
	343.82	
	349.62	

TABLE III
Transitions and Wavelengths of Molecular Emissions Observed [24]

Species	Wavelength (nm)	Transition
C_2	516.52	$A^3\Pi_g - X^3\Pi_u$
CH	431.42	$A^2\Delta - X^2\Pi$

The major atomic emission peaks and molecular band heads observed in this study are summarized in Tables II and III, respectively. The analog signals produced by optical channels are captured by an Ocean Optics ADC1000 high-speed ISA-bus A/D converter installed in a Pentium PC. The OES data are then transmitted through fast ethernet to the computer used for real-time process control.

IV. Feedback Control System: Design and Implementation

The carbon content of the thin film cannot be measured directly in real-time, and thus, estimates of the carbon content,

which are obtained based on plasma composition in the reactor chamber by OES, are used in the feedback control system. Previous spectroscopic study of the reaction plasma [15] in this ECR PECVD system has shown that the carbon content in the film has a quasilinear relationship with respect to the optical emission intensity ratio of C_2 molecules and O atoms in the reacting gas. This can be explained by the fact that carbon molecules are mostly responsible for forming the precursors for carbon incorporation into the film. This result suggests that the information of optical emission intensity ratio of C_2/O can be utilized to estimate the carbon content in the zirconium dioxide film in real time.

In this paper, a mathematical model is constructed to estimate the carbon content of the film based on the optical emission intensity ratio which is obtained through OES in real time. Following the previous experimental results [15], the relationship between the carbon content in the surface layer and the optical emission intensity ratio can be written as

$$X_C^s(t) = A\gamma(t) \tag{1}$$

where X_C^s is the atomic concentration (%) of carbon in the surface of the film, A is a constant which is related to the configuration and chamber condition of the specific experimental system (experimentally determined for our system to be 11.92), and γ is the optical emission intensity ratio of C_2/O.

The dominant factor that may lead to possible variation in the value of the parameter A is the chamber wall conditions. During the PECVD process, material deposition may occur on the substrate as well as on the reactor chamber wall. Although the deposition on the chamber wall is negligible compared to the deposition on the substrate for a single deposition experiment since the plasma is highly anisotropic, over time the accumulated coatings on the wall will change the chamber wall potential and may be sputtered off the wall onto the substrate, thereby, leading to a reactor chamber condition corresponding to a different value of A. However, in practice, for each deposition run the change of A is negligible under the range of operating conditions of our interest. Moreover, chamber cleaning is regularly scheduled to avoid material accumulation on the chamber wall. Thus, A can be considered constant for a well-maintained system (nevertheless, to implement the control system on another reactor, experimental calibration of the parameter A may be necessary).

Under the assumption that the film growth rate remains constant, the carbon content of the whole film is obtained using

$$X_{\mathrm{C}}(t) = \frac{\int_{t_0}^{t} X_{\mathrm{C}}^s(s)ds}{t - t_0} \tag{2}$$

where X_{C} is the atomic concentration (%) of carbon in the deposited film at time t and t_0 is the time in which the deposition starts. In this case, we treat X_{C} as the time average of X_{C}^s. Combining (1) and (2), the following estimation model is obtained:

$$X_{\mathrm{C}}(t) = A\frac{\int_{t_0}^{t} \gamma(s)\, ds}{t - t_0}. \tag{3}$$

We note that although the deposition process is a batch process in nature, an optimal operating recipe cannot be obtained since no accurate mathematical model describing the relationship between the optical emission intensity ratio and the inlet mass flow rate is currently available. Thus, the control problem for the process is formulated as a set-point regulation problem; this approach is further justified by our experimental results which clearly show that the response time of the closed-loop system is significantly smaller than the total deposition time.

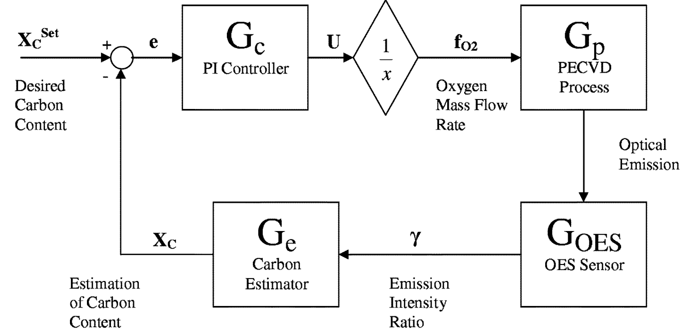

Fig. 3. Block diagram of the closed-loop system under the proposed carbon content controller.

Fig. 3 shows the structure of the closed-loop system under the proposed carbon content controller. The input to the controller is the difference between the desired carbon content and the estimated carbon content and the controller manipulates the inlet oxygen mass flow rate. The sensor block G_{OES} can be treated as a pure time delay since it takes a fixed amount of integration time for the OES system to obtain good signal-to-noise ratios and transfer the OES data through the network. The G_e block is the carbon estimator described above. The G_c block is the controller based on the proportional-integral (PI) control algorithm (described below in detail). The G_p block is the process block describing the relationship between the change of oxygen mass flow rate and the optical emission intensity ratio γ of the plasma. G_p is identified experimentally and the identification procedure will be discussed in detail in Section V-A.

The oxygen mass flow rate is chosen as the manipulated variable because it provides the most effective way to influence the gas phase composition and it does not disturb the plasma stability compared to other candidate manipulated variables such as the microwave power, the eletromagnetic field strength, the substrate temperature, and the chamber pressure. The argon mass flow rate is not selected as the manipulated variable because it significantly affects the film growth rate.

To eliminate unnecessary control actions, which may interfere with the plasma and lead to poor closed-loop performance, the control objective is to stabilize the carbon content value close to the desired set point (i.e., within a certain tolerance ϵ). A PI control algorithm is used of the following form:

$$\frac{1}{f_{\mathrm{O}_2}(t)} = U(t) = \frac{K_c\hat{e}(t) + K_i\int_{t_0}^{t}\hat{e}(\mu)d\mu + \bar{R}_f}{f_{\mathrm{Ar}}(t)} \tag{4}$$

$$\hat{e}(t) = \begin{cases} e(t) & |e(t)| > \epsilon \\ 0 & |e(t)| \leq \epsilon \end{cases} \tag{5}$$

where U is the output of the controller, f_{O_2} is the oxygen mass flow rate, f_{Ar} is the Argon mass flow rate which scales with the precursor vapor flow rate, $\bar{R}_f$ is a steady-state bias expressed in

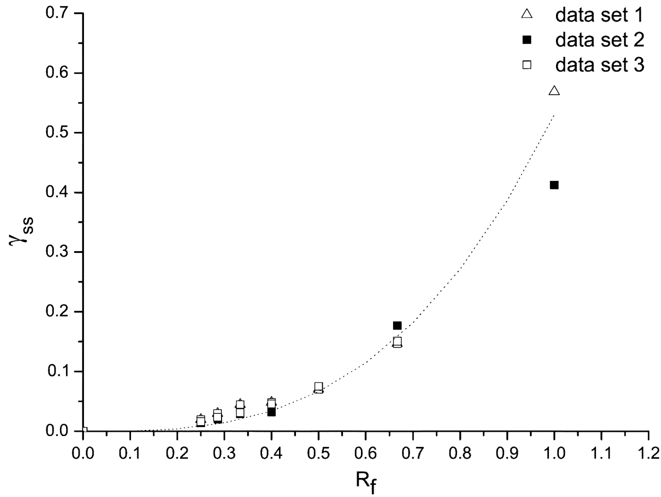

Fig. 4. Experimental data of R_f versus the γ_{ss} from different depositions for fixed argon flow rate 8 sccm, chamber pressure at 40 mtorr, and microwave power 300 W.

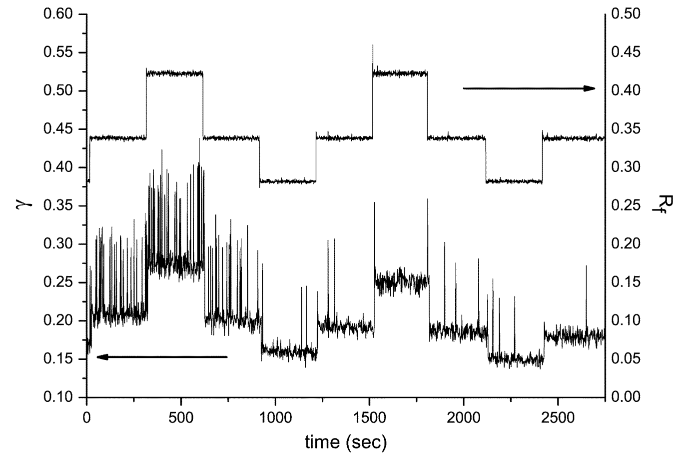

Fig. 5. Response curve of γ of step changes in R_f for argon flow rate 8 sccm, chamber pressure 40 mtorr, and microwave power 300 W.

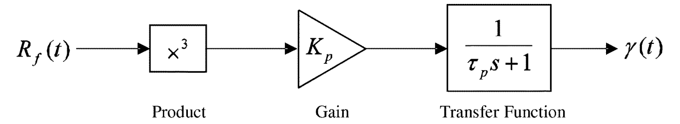

Fig. 6. Simulink representation for the process dynamics.

terms of the mass flow ratio of $\mathrm{Ar/O_2}$ at steady state, e is the difference between estimated carbon content and the set-point value, K_c is the proportional gain, and K_i is the integral gain. The input of the controller $\hat{e}(t)$ is defined as in (5) where ϵ is the tolerance within which we want to approach the desired set point.

MATLAB simulations of the entire process model are performed to obtain reference values of the controller parameters to be used in the real-time computer control system. The reference values are initially computed by using the Ziegler Nichols (ZN) tuning method (e.g., [20]) and then adjusted based on closed-loop simulation runs to achieve a desired output response.

The computer process control system was implemented on an Intel Pentium III 700 MHz PC with 512 MByte RAM. All the programs used in this study were written in LabVIEW language and National Instruments LabVIEW for Windows Version 6.1 was used as run-time platform.

V. Experimental Results and Discussion

A. Open-Loop System

The objective of the open-loop experiments is to study the dynamic behavior of the deposition process based on real-time OES measurements.

The first set of experiments (three independent runs) were performed to study the relationship between the steady-state value of γ and the mass flow ratio of $\mathrm{Ar/O_2}, R_f$. The experimental results are shown in Fig. 4; each data point is obtained by setting R_f at a fixed value and measuring γ after 200 s to guarantee that the process has reached steady state. The experimental results in Fig. 4 suggest that the optical emission intensity ratio varies proportionally with respect to the cubic of the mass flow rate ratio; this relationship is shown by the dotted line and can be mathematically expressed as

$$\gamma_{ss} = K_p R_f^3 \tag{6}$$

where γ_{ss} is the steady-state value of the optical emission intensity ratio and K_p is a constant which depends on the processing chamber conditions and the carrier gas flow rate.

In the second experiment, the process dynamics are identified by varying the mass flow ratio R_f in a way shown in the top curve in Fig. 5 and measuring γ in real time using OES; the experimental results are presented in Fig. 5. It can been seen that the process can be approximated by a first-order system which has a small time constant.

Using the experimental results shown in Figs. 4 and 5, we constructed a *Simulink* model shown in Fig. 6 within a MATLAB environment to obtain initial values of the controller parameters by simulation; $R_f(t)$ is the input and $\gamma(t)$ is the output. The model parameters were identified from the experiments to be $K_p = 0.53$ and $\tau_p = 10$ s.

Fig. 7 shows the evolution of the carbon concentration of the surface (A) and of the bulk (B) of a ZrO_2 film during a typical open-loop deposition. The carbon concentrations are computed based on real-time OES measurements using the proposed estimation model. It can be observed that the starting stage of the deposition has relatively higher carbon incorporation. This corresponds to the OES measured high C_2 emission intensity and low O emission intensity during the initial stage of the deposition, as shown in Fig. 8. Low O emission intensity indicates a low O concentration in the plasma; this may cause incomplete oxidation of the precursor, which leads to a high concentration of C_2 in the plasma during the initiation of the deposition process.

It can also be noticed in Fig. 7 that the carbon concentration of the bulk of the film changes throughout the deposition process. This is not only because the bulk carbon concentration is an average value, but also because the carbon incorporation rate varies with time. This time variation may be explained by the continuous increase of O concentration in the plasma due

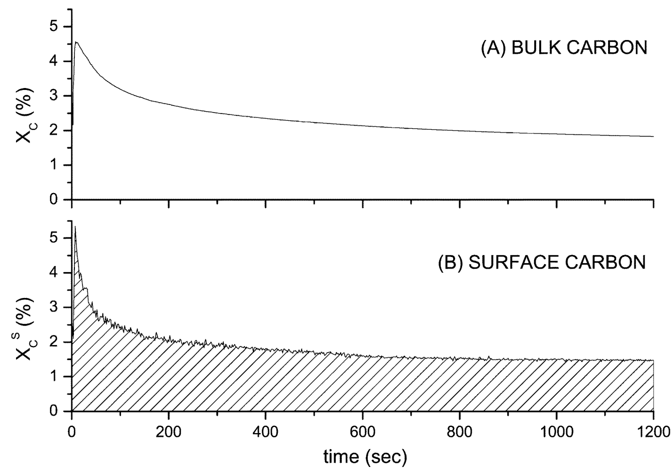

Fig. 7. Evolution of bulk (A) and surface (B) carbon concentration of a ZrO_2 film computed based on real-time OES measurements during an open-loop deposition with microwave power 300 W, chamber pressure 40 mtorr, Ar flow rate 8.4 sccm, and O_2 flow rate 8 sccm.

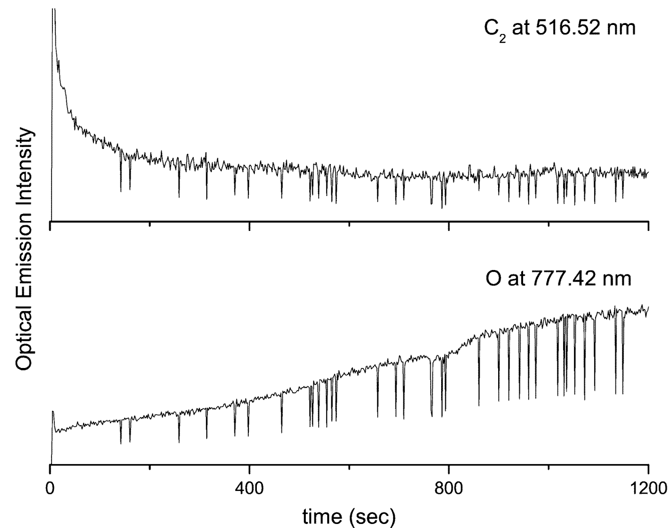

Fig. 8. Evolution of C_2 and O optical emission intensity during an open-loop deposition with microwave power 300 W, chamber pressure 40 mtorr, Ar flow rate 8.4 sccm, and O_2 flow rate 8 sccm.

to the complex and competing serial oxidation and dissociation processes [21]. As a result, reaction products with different compositions are generated and different amount of carbon is incorporated into the film at different times during the deposition process. Moreover, the magnitude of the carbon incorporation rate at the initial stage of the deposition is high and unpredictable (this may be due to the fact that the precursor feed rate which scales with the Ar flow rate is unpredictable as a result of the big pressure difference between the chamber and the bubbler at the beginning of the deposition), the variation would result in significant difference in the bulk carbon concentration, especially for an ultra thin film, since the total duration of the film deposition is quite short. Due to the existence of these uncertainties in the deposition process, the profile of bulk concentration of carbon shown in Fig. 7 is not reproducible in our experiments; this suggests that it is very difficult to obtain a desired carbon concentration with open-loop operation.

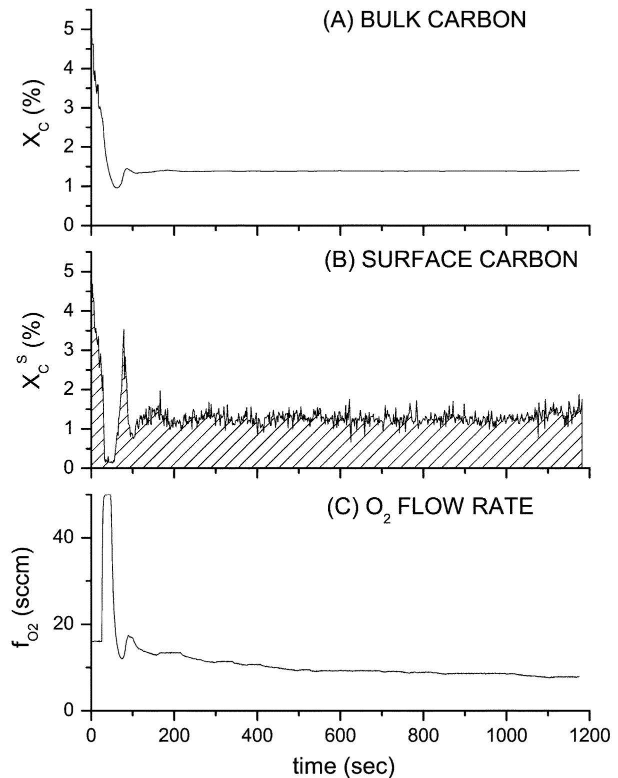

Fig. 9. Evolution of bulk (A) and surface (B) carbon concentration of a ZrO_2 film computed based on real-time OES measurements and profile of manipulated oxygen flow rate (C) during a controlled deposition experiment with microwave power 300 W, chamber pressure 40 mtorr and Ar flow rate 8.4 sccm.

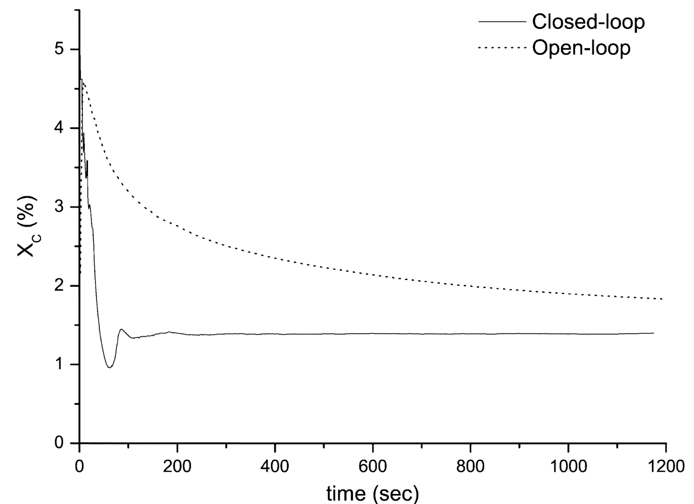

Fig. 10. Closed-loop deposition vs. open-loop deposition with same initial deposition condition of microwave power 300 W, chamber pressure 40 mtorr, Ar flow rate 8.4 sccm and O_2 flow rate 6 sccm.

B. Closed-Loop System

Using the developed real-time feedback control system, carbon content-controlled deposition experiments were performed. Fig. 9 shows a 20-min-long controlled-deposition which was carried out with microwave power fixed at 300 W, chamber pressure controlled at 40 mtorr and Ar flow rate set at

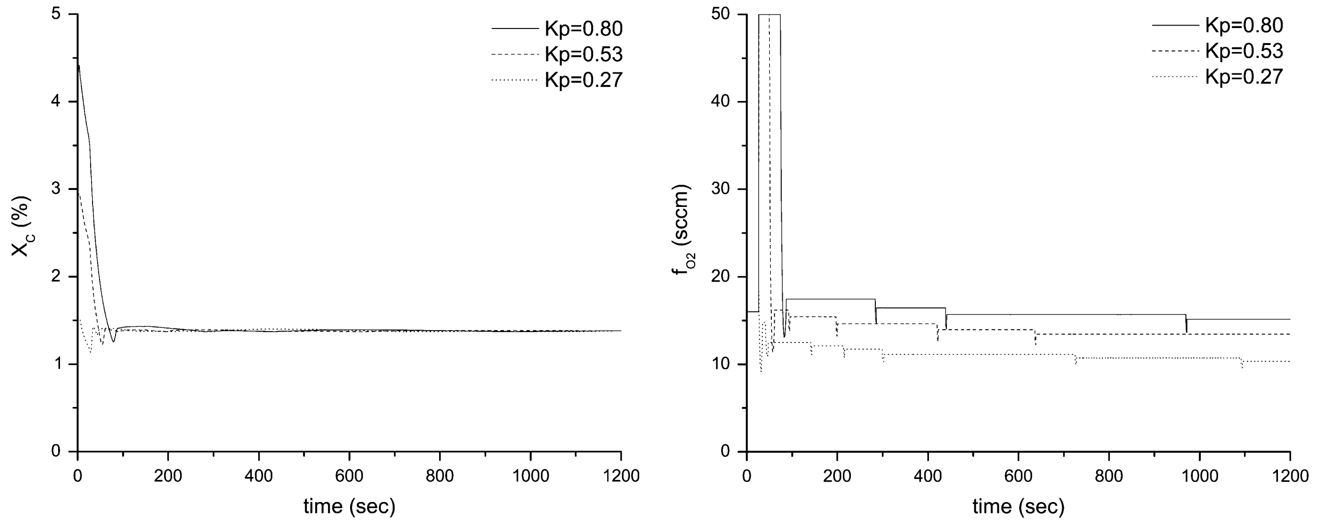

Fig. 11. Simulated profiles of X_C (left) and f_{O_2} (right) of the closed-loop system with $K_p = 0.27$ (dotted line), $K_p = 0.53$ (dashed line) and $K_p = 0.80$ (solid line).

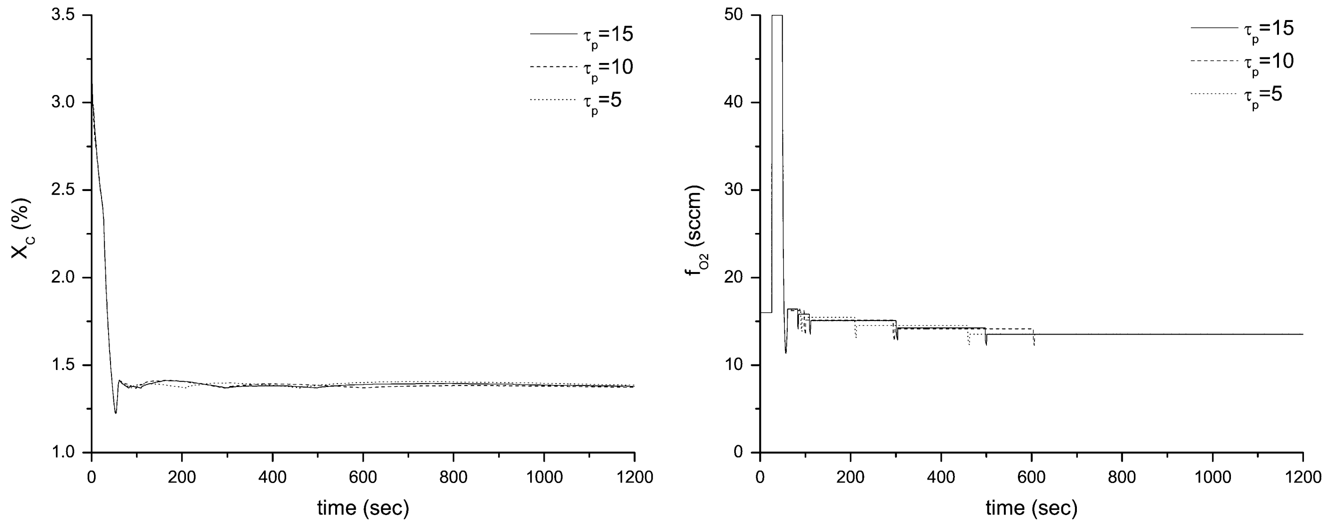

Fig. 12. Simulated profiles of X_C (left) and f_{O_2} (right) of the closed-loop system with $\tau_p = 5$ (dotted line), $\tau_p = 10$ (dashed line), and $\tau_p = 15$ (solid line).

8 sccm. The carbon content controller was implemented with a set-point value for the atomic carbon concentration of 1.4%, proportional gain $K_c = 1.0$, integral gain $K_i = 0.05$ and error tolerance $\epsilon = 0.03\%$.

From the bulk carbon concentration curve in Fig. 9, we can see that the carbon content of the film was controlled very closely to the desired value of 1.4% in spite of the initial plasma disturbance mentioned above (this result was also verified through off-line XPS analysis of the deposited film shown in Fig. 16). The response time is relatively small compared to the deposition duration which supports our set-point regulation formulation of this control problem.

A comparison of the bulk carbon concentration profile of the thin films under closed-loop (Fig. 9) and open-loop (Fig. 7) conditions with the same initial deposition conditions is shown in Fig. 10. It can be clearly seen that the carbon content of the film was reduced by more than a factor of 5 under closed-loop control.

Moreover, to examine the robustness of the closed-loop system, we modify the set-point of the Ar mass flow controller so that the actual $f_{\rm Ar}$ is 5% higher than its nominal value. We observed in the XPS compositional analysis that the sample deposited under open-loop conditions has slightly higher carbon due to the variation in $f_{\rm Ar}$, while the sample deposited under closed-loop operation has a carbon content that is very close to the desired set-point value (within the error range of XPS compositional analysis, which is about ± 0.1 atomic percent). This result clearly demonstrates that closed-loop operation has better tolerance to process disturbances than open-loop operation, and thus, with currently available equipment, closed-loop operation is expected to reduce thin film variability, which is the result of variation in the operating conditions.

Because the controller parameters are determined based on computer simulation using the identified values for the process

TABLE IV
XPS ATOMIC SENSITIVITY FACTORS (ASFs)

Species	Wavelength (nm)	Transition
C_2	516.52	$A^3\Pi_g - X^3\Pi_u$
CH	431.42	$A^2\Delta - X^2\Pi$

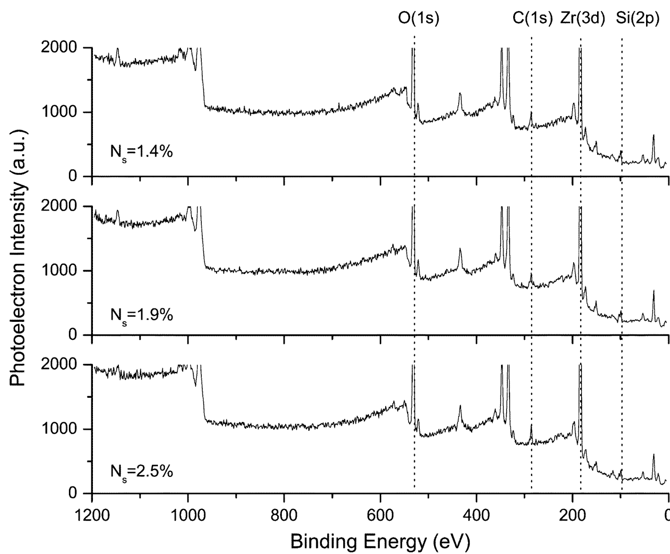

Fig. 13. XPS survey spectra obtained from ZrO_2 thin films deposited by closed-loop depositions with set-point values of 1.4%, 1.9%, and 2.5%.

parameters K_p and τ_p, we have also tested the sensitivity of the closed-loop system with respect to variations on the values of K_p and τ_p. Since the experimentally determined variations of K_p and τ_p in the range of operating conditions of interest are within the same order of magnitude, closed-loop simulations in which K_p and τ_p are varied by $\pm 50\%$ have been performed. In these simulations, the set-point of the bulk carbon content is fixed at the original value (1.4%) and the controller parameters determined for the original process model ($K_p = 0.53, \tau_p = 10$), $K_c = 1.0$ and $K_i = 0.05$, have been used in all scenarios. Figs. 11 and 12 show the profiles of the controlled variable X_C and manipulated variable f_{O_2} for varying K_p and τ_p respectively. It can be seen that the stability of the closed-loop system is not affected by the variations in either K_p or τ_p and there are no significant deteriorations in the achievable closed-loop output response.

C. XPS Analysis

The X-ray photoelectron spectra were obtained by a VG ESCALAB 5 electron spectrometer using an Al Kα X-ray radiation source (1486.6 eV). The take-off angle of 90° was used in all analysis. Survey scans ranging from 10 to 1200 eV were recorded using 1-eV step and 50-eV electron analyzer pass energy. High-resolution regional spectra of main elemental constituents are recorded using 0.1-eV step and 20-eV electron analyzer pass energy. The sampling depth is approximately 5–6 nm. The pressure in the analysis chamber is in the 10^{-10} torr range. The measured binding energy data were referenced to the surface C(1s) peak at 285 eV [22]. Atomic sensitivity factors used for the computation of the concentration of elements of interest are listed in Table IV.

Fig. 13 shows the survey spectra obtained from ZrO_2 thin films deposited by closed-loop operations with set-point values of 1.4% (top), 1.9% (middle), and 2.5% (bottom). The thickness of all the deposited films was within the sampling depth of the XPS system since Si(2p) substrate peaks were observable in all spectra.

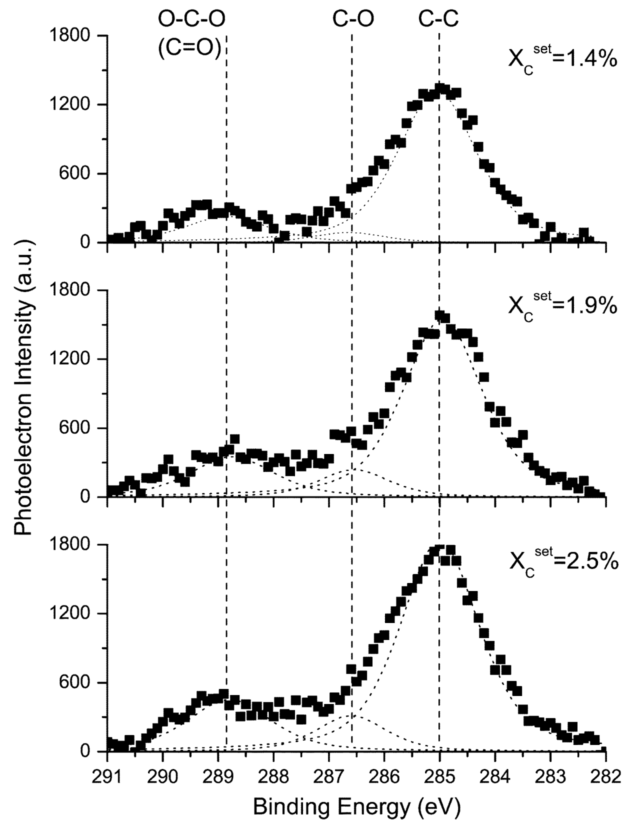

Fig. 14. Carbon 1s peaks of the XPS spectra obtained from ZrO_2 thin films deposited by closed-loop depositions with set-point values for carbon content of 1.4%, 1.9%, and 2.5%.

Fig. 14 shows the carbon 1s peaks of the XPS spectra obtained from ZrO_2 thin films deposited by closed-loop depositions with set-point values of 1.4%, 1.9% and 2.5%. The deconvoluted C(1s) peaks at 285.0, 286.6 and 288.8 eV shown as dotted lines in Fig. 14 are attributed to C-C, C-O and O-C-O (or C = O) bonds, respectively. From our previous work, we confirmed that most of the C-C incorporation comes from the ambient contamination to the film surface during sample transfer from the PECVD system to the XPS system, and thus, the amount of C-C bonds is not accounted for in the compositional analysis. The area of carbon-oxygen peaks in the XPS spectra is considered as a measure of the amount of carbon incorporation into the ZrO_2 films.

A comparison of the deconvoluted carbon-oxygen peaks from ZrO_2 films obtained by closed-loop depositions with different set-points is shown in Fig. 15. It is evident that the lower the carbon content set-point in the controlled-deposition, the smaller the peak area for both carbon oxidation states, which is a good demonstration of the effectiveness of the real-time carbon content control system on the ZrO_2 thin-film deposition.

The actual carbon concentration as well as the O/Zr ratio of ZrO_2 thin films from closed-loop deposition with different carbon content set-point values are computed from XPS spectra and presented in Fig. 16. The C-C peaks which were considered as ambient contamination were removed from the calculations. The O/Zr ratio was computed by subtracting the O-C bonds to obtain the actual stoichiometric ratio of ZrO_2 in the film. The

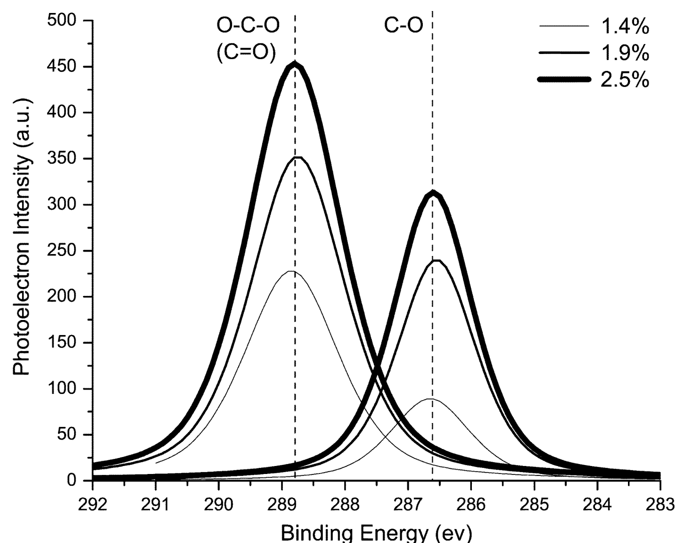

Fig. 15. Comparison of deconvoluted carbon-oxygen peaks in C(1s) XPS spectra obtained from ZrO_2 thin films deposited by closed-loop operation with set-point values of 1.4%, 1.9%, and 2.5%.

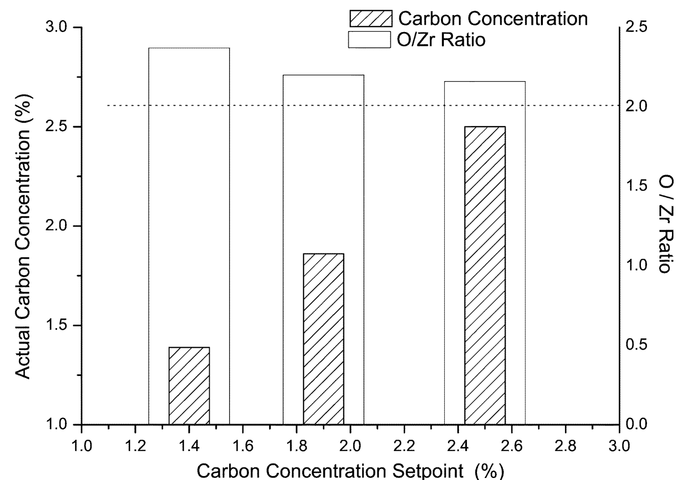

Fig. 16. XPS compositional analysis results for closed-loop deposited ZrO_2 thin films.

actual carbon concentration of the closed-loop deposited films matches quite well with the corresponding set-point values. The O/Zr ratios for all the films are greater than 2, which implies that fully stoichiometrically grown ZrO_2 films were deposited. The O/Zr ratios are slightly higher than 2; this is due to the fact that a small portion of the measured O(1s) intensity was due to O-H bonds whose binding energies were indistinguishable from the O-Zr bonds in the XPS analysis.

VI. Conclusion

In this work, a method for real-time control of thin film composition in a PECVD process using combination of on-line OES and off-line XPS was presented. The method was used for real-time carbon content control of ZrO_2 thin films. An estimation model of carbon content of ZrO_2 thin films based on real-time optical emission spectroscopy data was initially developed. A feedback control scheme, which employs the proposed estimation model and a proportional-integral controller, was designed to achieve carbon content control. Based on this methodology, a real-time control system was developed and implemented on an experimental ECR PECVD system. Experimental results of depositions and XPS analysis of deposited thin films under both open-loop and closed-loop operations were shown and compared. The advantages of operating the process under real-time feedback control in terms of robust operation and lower carbon content were demonstrated.

References

[1] H. Iwai and H. S. Momose, "Ultra-thin gate oxides performance and reliability," *IEDM Tech. Dig.*, pp. 163–166, 1998.

[2] S. H. Lo, D. A. Buchanan, Y. Taur, and W. Wang, "Quantum-mechanical modeling of electron tunneling current from the inversion layer of ultra-thin-oxide nMOSFETs," *IEEE Electron Device Lett.*, vol. 18, pp. 209–211, 1997.

[3] M. Copel, M. Gribelyuk, and E. Gusev, "Structure and stability of ultra-thin zirconium oxide layers on Si(001)," *Appl. Phys. Lett.*, vol. 76, pp. 436–438, 2000.

[4] C. Chaneliere, J. L. Autran, R. A. B. Devine, and B. Balland, "Tantalum pentoxide (Ta_2O_5) thin films for advanced dielectric applications," *Mater. Sci. Eng., R.*, vol. 22, pp. 269–322, 1998.

[5] C. Vahlas, F. Maury, and L. Gueroudji, "A thermodynamic approach to the CVD of chromium and of chromium carbides starting from $Cr(C_6H_6)_2$," *Chem. Vap. Deposition*, vol. 4, pp. 69–76, 1998.

[6] F. Maury, L. Gueroudji, and C. Vahlas, "Selection of metalorganic precursors for MOCVD of metallurgical coatings: Application to Cr-based coatings," *Surf. Coat. Technol.*, vol. 87, pp. 316–324, 1996.

[7] A. Armaou and P. D. Christofides, "Plasma-enhanced chemical vapor deposition: Modeling and control," *Chem. Eng. Sci.*, vol. 54, pp. 3305–3314, 1999.

[8] A. Armaou, J. Baker, and P. D. Christofides, "Feedback control of plasma etching reactors for improved etching uniformity," *Chem. Eng. Sci.*, vol. 56, pp. 1467–1475, 2001.

[9] P. D. Christofides, *Nonlinear and Robust Control of Partial Differential Equation Systems: Methods and Applications to Transport-Reaction Processes*. Boston, MA: Birkhäuser, 2001.

[10] Z. H. Zhou and R. Reif, "Epi-film thickness measurements using emission fourier transferm infrared spectroscopy—Part II: Real-time in situ process monitoring and control," *IEEE Trans. Semiconduct. Manufact.*, vol. 8, p. 340, Aug. 1995.

[11] T. J. Knight, D. W. Greve, X. Cheng, and B. H. Krogh, "Real-time multivariable control of PECVD silicon nitride film properties," *IEEE Trans. Semiconduct. Manufact.*, vol. 10, p. 137, Feb. 1997.

[12] J. W. Coburn and M. Chen, "Optical emission spectroscopy of reactive plasmas: A method for correlating emission intensities to reactive particle density," *J. Appl. Phys.*, vol. 51, no. 6, p. 3134, 1980.

[13] C. Rebholz, J. Schneider, H. Ziegele, B. Rahle, A. Leyland, and A. Matthews, "Deposition and characterization of carbon-containing tungsten coatings prepared by reactive magnetron sputtering," *Vacuum*, vol. 49, no. 4, p. 265, 1998.

[14] I. L. Eisgruber, J. R. Engel, R. E. Hollingsworth, P. K. Bhat, and R. Wendt, "Intelligent process control of indium tin oxide sputter deposition using optical emission spectroscopy," *J. Vac. Sci. Tech. A*, vol. 17, no. 1, p. 190, 1999.

[15] B. O. Cho, S. Lao, L. Sha, and J. P. Chang, "Spectroscopic study of plasma using zirconium tetra-tert-butoxide for the plasma enhanced chemical vapor deposition of zirconium oxide," *J. Vac. Sci. Tech. A*, vol. 19, no. 6, p. 2751, 2001.

[16] Y. Ide, H. Era, and K. Kishitake, "Formation and properties of cr-n films by dc reactive sputtering," *J. Jpn. Inst. Metals*, vol. 65, no. 6, p. 502, 2001.

[17] Y. Lou and P. D. Christofides, "Estimation and control of surface roughness in thin film growth using kinetic Monte-Carlo models," *Chem. Eng. Sci.*, vol. 58, pp. 3115–3129, 2003.

[18] ——, "Feedback control of growth rate and surface roughness in thin film growth," *AIChE J.*, vol. 49, pp. 2099–2113, 2003.

[19] H. J. Frenck, E. Oesterschulze, R. Beckmann, W. Kulisch, and R. Kassing, "Low temperature remote plasma-enhanced deposition of thin metal oxide films by decomposition of metal alkoxides," *Mater. Sci. Eng. A*, vol. 139, pp. 394–400, 1991.

[20] D. R. Coughanowr, *Process Systems Analysis and Control*. New York: McGraw-Hill, 1991.

[21] B. O. Cho, J. Wang, and J. P. Chang, "Metalorganic precursor decomposition and oxidation mechanisms in plasma-enhanced ZrO_2 deposition," *J. Appl. Phys.*, vol. 92, no. 8, p. 4238, 2002.

[22] *Handbook of X-Ray Photoelectron Spectroscopy: A Reference Book of Standard Spectra for Identification and Interpretation of XPS Data*, Perkin-Elmer, Physical Electronics Division, 1992. J. F. Moulder, K. D. Bomben, P. E. S. W. F. Stickle, and J. Chastain.

[23] A. R. Striganov and N. S. Sventitskii, *Tables of Spectral Lines of Neutral and Ionized Atoms*. New York: IFI/Plenum, 1968.

[24] R. W. B. Pearse and A. G. Gaydon, *The Identification of Molecular Spectra*. New York: Wiley, 1976.

Dong Ni, photograph and biography not available at the time of publication.

Yiming Lou, photograph and biography not available at the time of publication.

Panagiotis D. Christofides, photograph and biography not available at the time of publication.

Lin Sha, photograph and biography not available at the time of publication.

Sandy Lao, photograph and biography not available at the time of publication.

Jane P. Chang, photograph and biography not available at the time of publication.